

Hypergraph Multi-modal Large Language Model: Exploiting EEG and Eye-tracking Modalities to Evaluate Heterogeneous Responses for Video Understanding

Minghui Wu^{1,2,3*} Chenxu Zhao^{2,3*} Anyang Su^{2,3*} Donglin Di³ Tianyu Fu³
 Da An³ Min He² Ya Gao^{1,2} Meng Ma¹ Kun Yan^{1†} Ping Wang^{1†}
¹Peking University ²Mininglamp Technology ³Shanghai Artificial Intelligence Laboratory

{wuminghui, zhaochenxu, suanyang, hemin}@mininglamp.com, gaoya@stu.pku.edu.cn, {mameng, kyan2018, pwang}@pku.edu.cn

Abstract

Understanding of video creativity and content often varies among individuals, with differences in focal points and cognitive levels across different ages, experiences, and genders. There is currently a lack of research in this area, and most existing benchmarks suffer from several drawbacks: 1) a limited number of modalities and answers with restrictive length; 2) the content and scenarios within the videos are excessively monotonous, transmitting allegories and emotions that are overly simplistic. To bridge the gap to real-world applications, we introduce a large-scale *Subjective Response Indicators for Advertisement Videos dataset*, namely SRI-ADV. Specifically, we collected real changes in Electroencephalographic (EEG) and eye-tracking regions from different demographics while they viewed identical video content. Utilizing this multi-modal dataset, we developed tasks and protocols to analyze and evaluate the extent of cognitive understanding of video content among different users. Along with the dataset, we designed a *Hypergraph Multi-modal Large Language Model (HMLLM)* to explore the associations among different demographics, video elements, EEG and eye-tracking indicators. HMLLM could bridge semantic gaps across rich modalities and integrate information beyond different modalities to perform logical reasoning. Extensive experimental evaluations on SRI-ADV and other additional video-based generative performance benchmarks demonstrate the effectiveness of our method. The codes and dataset will be released at <https://github.com/suay1113/HMLLM>.

1. Introduction

With the advancement of Large Language Models (LLMs) [69] and Multi-modal Large Language Models [11, 31, 43,

* Authors contributed equally to this work.

† Corresponding authors.

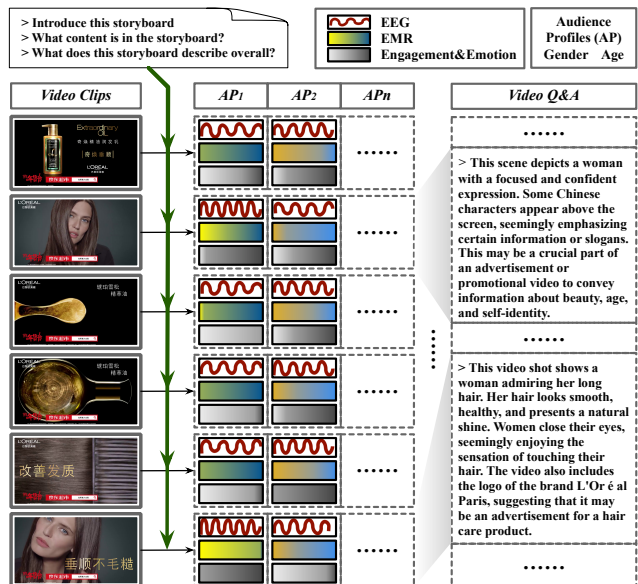


Figure 1. Our proposed Subjective Response Indicators for Advertisement Videos (SRI-ADV) dataset. Real-time signals captured by electroencephalographic (EEG) and eye-tracking devices reveal that Audience Profiles (AP) of varying genders and ages exhibit distinct engagements, emotions, and eye motion ratios (EMR) when exposed to various scenes and elements within the same advertisement video.

44], the field of video understanding has entered a new era. The advanced logical reasoning abilities of multi-modal LLMs facilitate a thorough analysis of explicit elements within videos. Moreover, these models can deduce the underlying implicit content of these explicit factors, leveraging the knowledge and experience acquired by LLMs. Existing benchmarks for video content question-and-answering, such as [30, 50, 72, 72, 76], provide a rich set of instruction labels. Alternatively, they exhibit several deficiencies as illustrated in Table 1: 1) the video content itself is overly simplistic, often only involving objective,

Table 1. Comparison of existing VideoQ&A datasets with ours (OE: open-ended, MC: multiple-choice, AP: Audience Profiles).

Datasets	Video source	Q&A generation	Q&A tasks	Modality	Videos	Q&A pairs	AvgAnsLen	MedScene
MSVD-QA [72]	MSVD	Auto	OE	Video	1,970	50,505	1.0	2
MSRVTT-QA [72]	MSRVTT	Auto	OE	Video	10,000	243,680	1.0	3
TGIF-QA [30]	TGIF	Auto&Human	OE & MC	Frame/Video	56,720	103,919	1.5	1
ActivityNet-QA [76]	ActivityNet	Human	OE	Video	5,800	58,000	1.3	7
Video-ChatGPT [50]	ActivityNet	Auto&Human	OE	Video	200	2,994	51.0	6
SRI-ADV-QA (ours)	Custom	Auto&Human	MC & OE	Video/EEG/EMR/AP	498	178,547	99.6	11

explicit factors, which does not support the exploration of deeper levels of video creativity and implicit factors. We utilize the **MedScene** metric to evaluate this issue, where **MedScene** denotes the median number of scene across all videos in the dataset. A higher number of scenes indicates greater complexity in video content; 2) the number of modalities included in these datasets are limited, generally confined to videos and frames; 3) the instruction labels concerning the length of answers are restricted to certain predetermined options, failing to assess the divergent and analytical abilities of LLMs. We utilize the **AvgAnsLen** to evaluate this issue, where **AvgAnsLen** represents the average text length of the answer portion across all Q&A pairs in the dataset. To address the issues mentioned above, we have prepared an extensive collection of content-rich advertisement videos, accompanied by a more comprehensive set of modality labels.

In the burgeoning field of cognitive neuroscience, the exploration of how individuals perceive and interpret video content has opened new avenues for understanding the intricate interplay between brain activity and media interaction [64]. Recent advancements in multi-modal data analysis have underscored the importance of leveraging diverse physiological signals to gain insights into the cognitive and emotional states of viewers [35]. Among these, Electroencephalographic (EEG) signals with their high temporal resolution, provide a direct measure of brain activity [56], capturing the nuanced and dynamic changes in cognitive states as individuals engage with video content. These signals embody the electrical manifestations of the brain’s complex neural dynamics, offering insights into the emotional and cognitive processes underpinning video content interpretation [55].

Inspired by the aforementioned context, we have utilized EEG and eye-tracking apparatus to collect and record the EEG and eye movement responses of individuals across various ages, genders, and professions while watching the same advertisement video. We aggregated this information into modality labels, introducing a novel, large-scale benchmark: the Subjective Response Indicators for Advertisement Videos dataset, namely **SRI-ADV**. As illustrated in Figure 1, our proposed dataset captures the subjective reactions of individuals watching videos through EEG and eye-tracking devices, fills the gaps in the video understand-

ing domain regarding the assessment of video appeal and implicit factors. How to effectively leveraging these multi-modal labels to uncover the latent associations among the modalities becomes the cornerstone for addressing deeper challenges in video understanding.

Graph-based methodologies exhibit superiority in exploring the associations among features, particularly hypergraphs, extending beyond traditional graph theory, offer a powerful framework for representing complex relationships in data [6]. In the context of video content analysis, hypergraphs can encapsulate the intricate associations among video elements, EEG signals, and eye-tracking data, allowing for the modeling of higher-order interactions that are not capturable through simple pairwise connections.

Utilizing the multi-modal information of the SRI-ADV dataset, coupled with the superiority of constructing associative features through hypergraph, we proposed a Hypergraph Multi-modal Large Language Model (**HMLLM**), integrating information from disparate modalities to perform logical reasoning and semantic analysis. By leveraging the rich information encoded in video content, along with EEG and eye-tracking data, HMLLM can bridge semantic gaps across modalities, offering a comprehensive understanding of the cognitive processes involved in video content interpretation.

The main contributions can be summarized as follows:

1. Introduction of a novel large-scale benchmark dataset: the Subjective Response Indicators for Advertisement Videos (SRI-ADV) dataset, a large-scale benchmark that captures real-time EEG and eye-tracking data from a diverse demographic while they watch advertisement videos. This dataset fills a significant gap in the field of video understanding by providing rich modality information and a comprehensive set of question-and-answer (Q&A) pairs that allow for the assessment of video creativity and implicit factors.
2. Development of the Hypergraph Multi-modal Large Language Model (HMLLM): we have developed a novel HMLLM that leverages the complex relationships among video elements, EEG signals, and eye-tracking data encapsulated in hypergraphs.
3. Extensive experimental evaluations demonstrating our method’s effectiveness: through rigorous experimental evaluations conducted on the SRI-ADV dataset and addi-

tional video Q&A datasets, we have demonstrated the effectiveness of our HMLLM.

2. Background

2.1. Video Understanding

Video understanding aims to create algorithms that allow machines to interpret videos with the same expertise as humans. Meanwhile, video emotion recognition [42][54][81] emphasizes the interplay between the emotions conveyed by the video and the viewer responses, collectively forming a critical component of video understanding. Most existing works focus on modeling objective and tangible visual properties of videos [16], particularly in action recognition [3, 7, 10, 17, 19, 20, 51, 58, 66, 68] and temporal action localization/detection [18, 46, 83]. However, the need for content recommendation systems has spurred research into subjective and intangible aspects (e.g. the appeal and memorability of content [14]), where various semantically rich information are considered [5, 13, 52, 82].

Compared with the above work, we present a new large-scale dataset filled with content-rich advertisement videos. This dataset includes a wider range of labels that cover both tangible and intangible aspects of content. Leveraging this dataset, we introduce an advanced hypergraph multi-modal large language model. This model is designed to simultaneously process various modalities, enabling it to conduct logical reasoning and perform in-depth semantic analysis of video content.

2.2. EEG-Based Emotion Recognition

Electroencephalography (EEG) signals provide detailed insights into brain activity related to emotions, offering spatial information on specific brain regions involved [8]. The Arousal-Valence model [57] is a key framework for classifying emotions along two dimensions. Xiaolin et al [60] explored various features to enhance the emotion recognition model. However, there’s a shift towards deep learning due to the limitations of machine learning. The dynamical graph convolutional neural network (DGCNN) [59] was proposed to learn discriminative EEG features and interrelationships among EEG channels. Some works have moved towards multi-modal learning for robust results in EEG signal recognition tasks, such as integrating physiological signals in the multi-modal framework to enhance emotion recognition accuracy [71] and employing proper windowing and channel selection to avoid relying on the full length of EEG and EOG signals for classification [9]. Furthermore, advancements in neuromorphic computing led to the use of Spiking Neural Networks (SNN) [49] for classifying spatiotemporal EEG data with lower computational requirements [33].

2.3. Multi-modal Large Language Models

Multi-modal Large Language Models (MLLMs), primarily serving as vision-language models, transform images or videos into texts. These models are mainly divided into two categories: traditional large-scale pretraining [37, 38, 65] and instruction tuning using pre-trained LLMs [47, 75, 84]. The first category comprises models that blend a visual encoder with a language model, either developed from scratch or based on pre-existing models, possibly including a trainable module to bridge the two modalities. Utilizing autoregressive loss for text generation, these models are training on extensive image-text datasets, including image-text pairs [28, 37, 38, 65] and image-text sequence instances [2]. The second category, drawing inspiration from instruction-tuning techniques used in MLLMs [1, 53], incorporates instruction-following data to enhance MLLMs’ zero- and few-shot learning abilities [15, 47, 75, 84]. A notable example is LLaVA [47], which employs a simple projection matrix to link a pre-trained visual encoder with an LLM, focusing initially on pre-training for feature alignment before comprehensive end-to-end fine-tuning. Some other works extend to video understanding by connecting video encoders to MLLMs [39, 45, 74, 78]. In addition to models that focus on combining images or videos with text, there are projects that incorporate even more types of data, like speech, audio, and sensor information [25, 61, 70, 77].

2.4. Hypergraph Learning

A hypergraph includes vertices and hyperedges, where hyperedges can connect multiple vertices. This structure is more adaptable and effective for representing complex relationships in data than traditional graphs [24]. Methods for creating hypergraphs fall into two groups: explicit and implicit. Explicit methods directly use the data structure to form hyperedges, like connecting vertices with shared attributes [27, 32]. Implicit methods, however, infer hyperedges from data without clear high-order links, utilizing approaches based on distance [22] or representations [48, 67]. Unlike static structures, some methods allow for hypergraph structure optimization, adjusting it during the learning phase. This involves adaptively changing weights on hyperedges [23] or sub-hypergraphs [80] to improve learning outcomes. Recent advancements have introduced deep hypergraph representation learning, a new approach that mainly divides into spectral [21, 73] and spatial [4, 26] categories based on how hypergraph convolution operator is defined.

3. SRI-RAV Dataset

In this section, we present the Subjective Response Indicators for Advertisement Videos (SRI-ADV) dataset. The SRI-ADV dataset not only focuses on the Objectivity Task

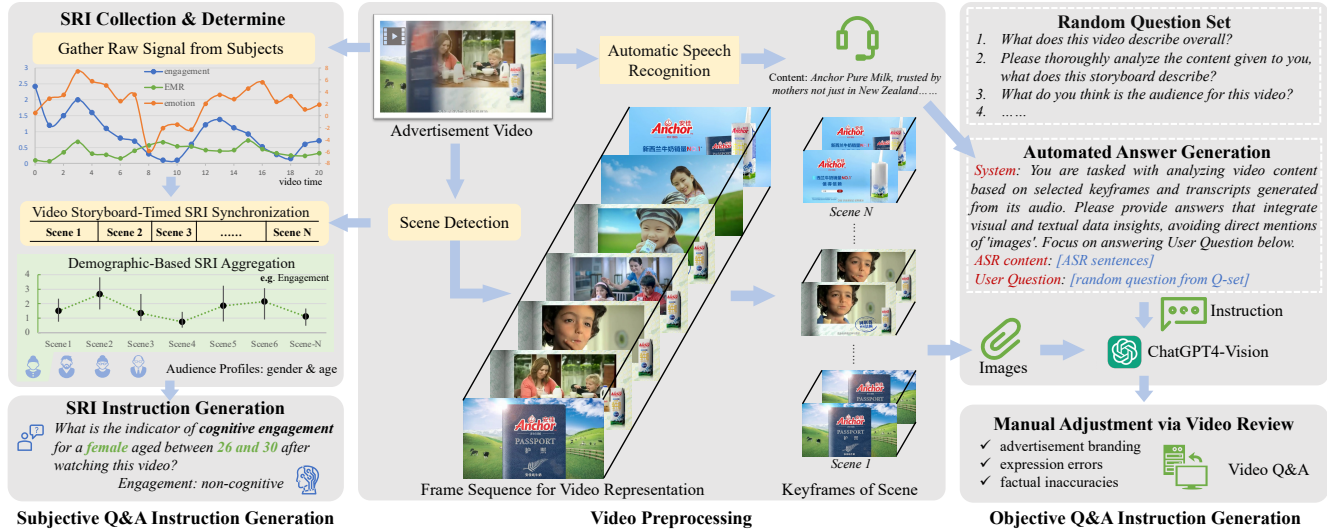


Figure 2. Generation pipeline of SRI-ADV dataset. The left side of this figure illustrates the process of SRI data collection, computation, and amalgamation. This involves acquiring raw signals from subjects, processing signals by video scenes, and pooling data from subjects with similar demographic profiles to obtain aggregated subjective response indicators and instruction for language models. The middle section depicts the video preprocessing with Frame Sequence for Video Representation (FSVR) by scene detection and Automatic Speech Recognition (ASR) for videos. On the right side, we present our proposed semi-automated video Q&A generation process, which leverages both video storyboarding from FSVR and dialogue text from ASR. This integration enriches video content comprehension, thereby facilitating both Subjectivity and Objectivity Tasks.

typically found in traditional video Q&A datasets but also meticulously collects subjective indices to enhance the richness. It encompasses a wide array of advertisement videos across different industries. To capture a diverse set of responses, we enlisted participants from various cities throughout Mainland China. These participants are equipped with EEG devices, enabling us to monitor their brainwave activities and eye motion ratios (EMR) in real-time while watching the advertisements. The collected data is subsequently analyzed to establish a benchmark for the classification of brainwave and EMR responses, which is elaborated in Sections 3.1 and 3.2.

Additionally, the SRI-ADV dataset includes an extensive video Q&A section to provide objective insights into the ads, facilitating model training and subjective index assessment. The task definition and protocol of our dataset are outlined in Section 3.3 and 3.4.

3.1. Frame Sequence for Video Representation

The SRI-ADV dataset features Chinese advertising videos from diverse fields such as food and beverages, household items, consumer electronics, cultural tourism, software, and automobiles. It comprises 498 curated landscape videos sourced from online platforms and TV commercial ads, each running for 15-30 seconds.

In this study, we introduce the Frame Sequence for Video Representation (**FSVR**) strategy to preprocess advertisement videos, as depicted in the middle part of Fig-

ure 2. We enhance the video scene sensitivity by integrating the AdaptiveDetector¹ for FSVR with specific parameters: `adaptive_threshold = 2`, `min_scene_len = 10`, `window_width = 2`. In the case of advertisement videos with frequent scene changes, the scene detection algorithm captures more information compared to average frame capture methods. Moreover, it is invaluable in minimizing redundant frames in videos primarily composed of static scenes.

By employing FSVR, we are able to deconstruct the temporal sequence of advertisement video frames, achieving capabilities including modality signal alignment, video content understanding, and semi-automated Q&A instruction generation.

3.2. Subjectivity: SRI Collection & Classification

We developed a sophisticated system for collecting subjective indicators. Each participant watches a series of advertisement videos using the device described in the appendix. During this process, we synchronously gather EEG and eye-tracking data, along with anonymized demographic details. Our study includes over 4,600 participants, ensuring a wide demographic representation. The diverse participant base spans white-collar workers, civil servants, students, and freelancers across various age groups and income brackets.

¹<https://www.scenedetect.com/>

The raw EEG signals are characterized by parameters such as $\alpha_1, \alpha_2 \dots \beta_2, \beta_3$ [34, 36], which is detailed in the appendix. Given the unique demands of advertisement video analysis, we pinpointed two pivotal EEG metrics: engagement and emotion, as delineated by Equation 1 and Equation 2, respectively.

$$EN_t = (\beta_2 + \beta_3) / (\alpha_3 + \alpha_2 + \beta_2 + \beta_3), \quad (1)$$

$$EM_t = (\alpha_3 - \alpha_2) / (\alpha_3 + \alpha_2) \times 100, \quad (2)$$

where EN_t and EM_t represent the engagement and emotion of the individual user at the sampling moment, respectively. Furthermore, we tracked eye movement data, defining the Eye Movement Ratio (EMR_t) as the proportion of time the participant’s gaze fixates on the display relative to the total video duration.

The SRI Collection & Determine workflow, depicted on the left of Figure 2, captures sub-second high-frequency raw signals data. To align with video content’s scene-based evolution, Video Storyboard-Timed SRI Synchronization was adopted, producing time-averaged and participant-specific SRIs. Demographic characteristics then grouped these SRIs into units of 5-20 same-gender participants with a maximum age difference of 5 years, such as {female, <20}, {male, 26-30}, and {female, 46-50}, as Demographic-Based SRI Aggregation in Equation 3.

$$\bar{X} = \frac{1}{P \cdot N} \sum_{i=1}^P \sum_{j=1}^N X_{p_i, t_j}, \forall p_i \in [AP], \forall t_j \in [t_1, t_2], \quad (3)$$

where X_{p_i, t_j} denotes the original Subjective Response Indicators such as EN_t , EM_t , and EMR_t . Each indicator associated with discrete values for participant p_i at specific timestamps t_j , where t_j signifies the effective sampling moment instances within the video storyboard timeframe from FSVR in Section 3.1.

For quantitative analysis, we meticulously examined data distribution across various Audience Profile segments. Engagement was categorized into two groups using the Leuven Engagement Scale (LES) and its distribution. Emotion and EMR indicators, which followed normal distributions, were divided into three equal categories. For detailed data distribution, refer to the appendix. The SRI Instruction Generation protocol is detailed in Table 2.

3.3. Objectivity: Semi-automated Generation

In addition to subjective indicators from Audience Profiles, we developed a semi-automated annotation pipeline for ChatGPT4-Vision (GPT4V) to obtain Objective Video Q&A, depicted in Figure 2. Although GPT4V cannot process videos, it supports multiple consecutive key-frames simultaneously. Based on FSVR in Video Preprocessing, we extracted middle frames from each shot as key-frames that

Table 2. Task and Protocol of SRI-ADV Dataset. In Task1, Protocol1 (**P1**) targets a broad audience. Protocol2 (**P2**), based on P1, contains SRI to Audience Profiles.

Task Name	1. Subjectivity	2. Objectivity
Eva. Form	Multi-classification	Text generation
Train Video	426	426
Test Video	72	72
Train Q&A	145,107	5762
Test Protocol	P1 P2	–
Test Q&A	2,640 26,724	954

effectively represent the entire video. During each invocation of GPT4V to automatically generate answers, questions are selected randomly from the Random Question Set to enhance the diversity of Q&A sessions, along with providing ASR text and FSVR key-frames. Lastly, annotators were carefully selected to manually refine objective Q&A instruction from Automated Answer Generation, addressing issues like advertisement branding, expression errors, and factual inaccuracies.

3.4. Data Overview, Tasks and Protocols

Based on the processing presented in Sections 3.2 and 3.3, SRI-ADV is categorized into subjectivity and objectivity tasks. The subjectivity task examines the SRI, whereas the objectivity task is dedicated to the qualitative analysis of video content and audience perception. As shown in Table 2, we present the tasks, protocols, and instructions associated with the SRI-ADV dataset.

Task 1, entitled **Subjectivity**, is formulated as a classification task, aimed at examining the influence of video content and user characteristics on the SRI. We develop two experimental protocols to guide this investigation. The first protocol (**P1**) is designed to assess the SRI ability of a broad audience, involving the analysis of average responses across different videos. This approach is relatively straightforward. The second protocol (**P2**) introduces a layer of complexity by focusing on the SRI discernment of particular user demographics. This necessitates a comprehensive examination of how response patterns fluctuate among diverse user cohorts.

Task 2, designated as **Objectivity**, mirrors the video Q&A tasks prevalent in prior datasets, as described in Section 3.3. Building on the method outlined in [50], this study conducts a supervised analysis of the answers generated, assessing their accuracy and allocating scores. This approach is designed to objectively ascertain the narrative coherence of the advertisement content and its efficacy in captivating the target audiences.

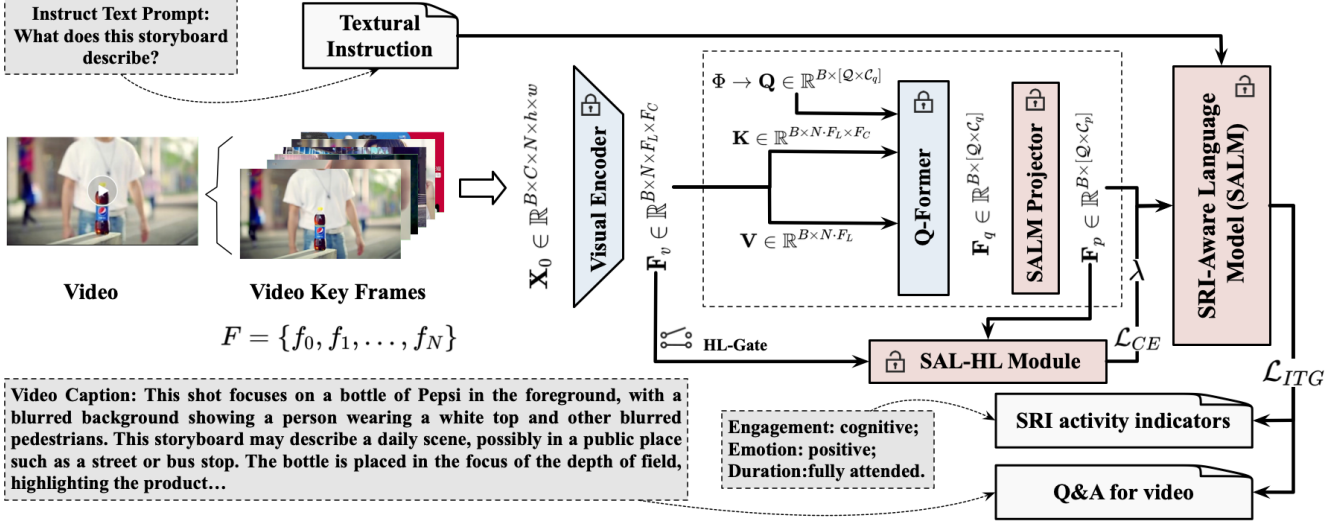


Figure 3. Overview of the Hypergraph Multi-modal Large Language Model (HMLLM). The architecture comprises a suite of pre-trained models, including a “Visual Encoder”, “Q-Former”, and the “SRI-Aware Language Model (SALM)”, which are initially frozen and subsequently fine-tuned through strategic training procedures. More importantly, our model incorporates a designed “SRI-Aware Language Hypergraph Learning (SAL-HL)” module that is trained de novo via a combined loss function. During inference, the HMLLM generates SRI and Q&A responses tailored to the video content, thereby providing a deeper level of engagement and comprehension.

4. Method

This section elaborates on the Hypergraph Multi-modal Large Language Model (HMLLM), an approach designed to intelligently process video clips and textual prompts for generating contextually relevant text, including Subjective Response Indicators (SRI). Central to our methodology are several key components as depicted in Figure 3: Visual Encoder, Query Former (Q-Former), SALM Projector, SRI-Aware Language Model (SALM), and SAL-HL Module. All components mentioned above synergistically orchestrated across two primary phases: SALM Warm-Up and SAL-HL Fine-Tuning, as depicted in our model architecture (refer to Figure 3). The pseudocode in the appendix illustrates the detailed training process.

4.1. SALM Warm Up

We begin by detailing the initial stage. The approach ingests brief video clips and corresponding textual prompts, extracting key frames from the videos using a predefined, static extraction strategy, which can be either random or uniformly distributed. These key frames are represented as $F = \{f_0, f_1, \dots, f_N\}$, with N signifying the number of extracted frames. These key frames are then pre-processed to form the initial data matrix, denoted by $\mathbf{X}_0 \in \mathbb{R}^{B \times C \times N \times h \times w}$, where B , C , N , h , and w correspond to the batch size, color channels (RGB), the number of keyframes, and the resized dimensions of the frames, respectively. The initial data matrix \mathbf{X}_0 is fed into a pre-trained visual encoder to yield initial visual representations, expressed as

$\mathbf{F}_v \in \mathbb{R}^{B \times N \times F_L \times F_C}$, with F_L and F_C representing the length and channels of features, respectively.

During the first training phase, the “Hypergraph Learning Gate (HL-Gate)” remains inactive while the Q-Former and SALM are warmed up. The visual features \mathbf{F}_v are then input into the frozen Q-Former as the **Key** ($\mathbf{K} \in \mathbb{R}^{B \times (N \times F_L) \times F_C}$) and **Value** ($\mathbf{V} \in \mathbb{R}^{B \times (N \times F_L)}$) for the attention mechanism. The **Query** in the Q-Former is initialized as either a random or null set, represented by $\mathbf{Q} \in \mathbb{R}^{B \times (Q \times C_q)}$, where $Q \times C_q$ are the predefined hyperparameters for the length and channels of the query. Subsequently, we introduce an “SALM Projector”, a multi-layer perceptron that follows the Q-Former, capable of reshaping the data and introducing additional learning parameters into the model. The output of projector is denoted as $\mathbf{F}_p \in \mathbb{R}^{B \times (Q \times C_p)}$, with C_p being another predefined hyperparameter. The SRI-Aware Language Model (SALM) is then engaged, taking the output of the SALM Projector (\mathbf{F}_p) and the corresponding textual instructions as inputs during the initial warm-up training stage. The SALM is trained using the **Image-grounded Text Generation (ITG)** loss function [38] (\mathcal{L}_{ITG}), which instructs the Q-Former to generate text conditioned on the input images. The goal of the ITG loss is to minimize the difference between the generated caption $\hat{Y}_{qa} \leftarrow \text{SALM}(\mathbf{F}_p, T)$ and the ground-truth caption Y_{gt} . This is typically achieved using a cross-entropy loss computed over the words or tokens in the caption. The

ITG loss function can be mathematically represented as:

$$\mathcal{L}_{ITG} = - \sum \left(\log \mathbb{P}(\mathbf{Y}_{gt_i} | \mathbf{Y}_{gt_1}, \dots, \mathbf{Y}_{gt_{i-1}}, \mathbf{F}_v) \right) \quad (4)$$

where $\mathbb{P}(\mathbf{Y}_{gt_i} | \mathbf{Y}_{gt_1}, \dots, \mathbf{Y}_{gt_{i-1}}, \mathbf{F}_v)$ denotes the probability of generating the i -th word in the caption given the previous words and the visual features extracted from the image. The summation encompasses all words or tokens in the ground-truth caption.

In our approach, we integrate specific strategies from BLIP2 [38] to address the limitation of Q-Former architecture on direct interactions between the image encoder and text tokens. Following the aforementioned training procedure, the SALM Projector and SALM are adequately warmed up, preparing them for subsequent fine-tuning optimization.

4.2. SAL-HL Fine-tune

In the subsequent fine-tuning phase, the hypergraph learning gate (HL-Gate) is activated, and the hypergraph learning module (SAL-HL) undergoes training in tandem with the fine-tuning of the SRI-Aware Language Model (SALM). As delineated in Figure 3, the SAL-HL module receives the initial visual features (\mathbf{F}_v) and the representations of the projected frames (\mathbf{F}_p) produced by the warmed SALM Projector as inputs.

The SAL-HL module initiates the process by merging these two feature sets (i.e., $\mathbf{F}_p, \mathbf{F}_v$) and then pooling them to generate frame-level representations ($\mathbf{F}_{frame.level}$). This process is formulated as:

$$\mathbf{F}_{frame.level} = \text{Pool}(\text{Feature_Mixer}(\mathbf{F}_p, \mathbf{F}_v)). \quad (5)$$

The *Feature_Mixer* denotes the mixing operation between two feature matrices, which can be implemented as a multi-layer perceptron (MLP). Each frame, denoted as f_i for $i \in [0, N]$, is considered a vertex (\mathcal{V}) within the hypergraph structure (\mathcal{G}), which facilitates the establishment of high-order relationships among the frames. The construction of the hypergraph entails the application of a clustering algorithm that links frames with similar latent visual features. After constructing the hypergraph, we proceed to train the Hypergraph Neural Network (HGNN) [21] in parallel with the Structured Attention Layer Mechanism (SALM). This process is mathematically formulated as follows:

$$\tilde{\mathcal{Y}}_{sri} = \sigma \left(\mathbf{D}_v^{-1/2} \mathbf{H} \mathbf{W} \mathbf{D}_e^{-1} \mathbf{H}^\top \mathbf{D}_v^{-1/2} \cdot \mathbf{F}_{frame.level} \cdot \Theta \right), \quad (6)$$

where $\tilde{\mathcal{Y}}_{sri}$ represents the predicted output from the SALM-enhanced HGNN, and σ denotes a non-linear activation function, which introduces the necessary non-linearity into the model for capturing complex patterns. $\mathbf{D}_e \in \mathbb{R}^{E \times E}$,

$\mathbf{D}_v \in \mathbb{R}^{N \times N}$, and $\mathbf{W} \in \mathbb{R}^{E \times E}$ denote the diagonal degree matrix of hyperedges, the degree matrix of vertices, and weight matrix of hyperedges, respectively. $\mathbf{H} \in \mathbb{R}^{N \times E}$ signifies the incidence matrix that connects hyperedges to their constituent vertices. $\sigma(\cdot)$ denotes the nonlinear activation function (e.g., LeakyReLU(\cdot)). Θ is a diagonal matrix representing the learnable parameters updated by the *Cross_Entropy* loss function in the fine-tuning loop. It functions similarly to a multilayer perceptron (MLP) layer. Finally, $\mathbf{F}_{frame.level}$ represents the input feature vectors associated with the vertices of the hypergraph. By employing this formulation, we effectively leverage the structural complexity of the hypergraph to enhance the learning capabilities of the HGNN, enabling it to capture and utilize the intricate relationships inherent within the data. This joint training regimen integrates two loss functions: the Cross-Entropy loss (\mathcal{L}_{CE}) and the Image-grounded Text Generation (ITG) loss from the prior stage. The combined loss function is expressed as:

$$\mathcal{L} = \mathcal{L}_{ITG} + \lambda \cdot \mathcal{L}_{CE}, \quad (7)$$

where λ is a hyperparameter that balances the influence of the Cross-Entropy loss and the ITG loss on the overall optimization process. This composite loss function ensures that the model not only generates text that is grounded in the visual content but also adheres to the learned high-order relationships within the hypergraph structure. This enhances the model’s capability to capture intricate interactions and dependencies among video frames.

5. Experiment

Metrics. In our study, the Subjectivity Task of SRI-ADV is structured in a multiple-choice question (MC) format. To evaluate its performance, we employ Accuracy (Acc) and F1 score as our metrics. For the zero-shot evaluation of the Subjectivity Task, we have devised a unique prompt, with detailed information provided in the appendix. The subsequent task, named Objectivity, involves open-ended (OE) text generation. For its evaluation, we introduce evaluation measures [50] based on assessments using GPT-3.5 Turbo.

Implementation Details. We employ UMT-L [41] as the visual encoder and Vicuna-7B-v0 [12] as the base model for the SRI-Aware Language Model (SALM). Following the methodology of BLIP2 [38], QFormer is configured with 64 queries. Throughout both the inference and training phases, we adhere to the FSVR strategy detailed in Section 3.1, which involves representing each video with 8 key frames. Further details of hypergraph construction can be found in the appendix.

Table 3. Results of different models on Subjectivity task (Engagement, Emotion, and EMR Duration). Using the Frame Sequence for Video Representation (FSVR) strategy is denoted by a "△".

Models	Protocol	Settings	Engagement (2 classes)		Emotion (3 classes)		EMR Duration (3 classes)	
			Acc	F1	Acc	F1	Acc	F1
Random	P1	—	50.44	49.93	32.30	26.26	35.01	32.10
	P2	—	50.14	50.00	33.13	33.03	33.52	33.18
GPT4V [△] [1]	P1	Zero-shot	58.57	71.95	52.46	50.67	49.94	53.43
	P2	Zero-shot	45.62	61.53	36.40	43.65	39.39	47.04
Gemini-pro-vision [△] [63]	P1	Zero-shot	59.89	73.70	17.66	20.00	46.40	47.96
	P2	Zero-shot	46.16	63.31	30.56	43.10	36.20	43.96
Video-LLaVA [45]	P1	Zero-shot	60.06	74.50	61.39	71.30	45.26	57.48
	P2	Zero-shot	46.38	61.38	31.04	42.71	31.56	49.30
Video-LLaVA [45]	P1	Finetune	66.29	66.85	72.33	81.94	61.05	61.80
	P2	Finetune	52.58	52.69	38.62	44.72	41.28	50.84
Video-Chat2 [40]	P1	Finetune	75.34	76.95	71.36	75.78	57.39	60.80
	P2	Finetune	60.06	60.02	39.66	40.24	44.06	45.51
HMLLM (Ours)	P1	Finetune	78.41	79.26	78.41	84.83	62.05	62.43
	P2	Finetune	64.43	64.65	43.20	48.84	51.96	56.24

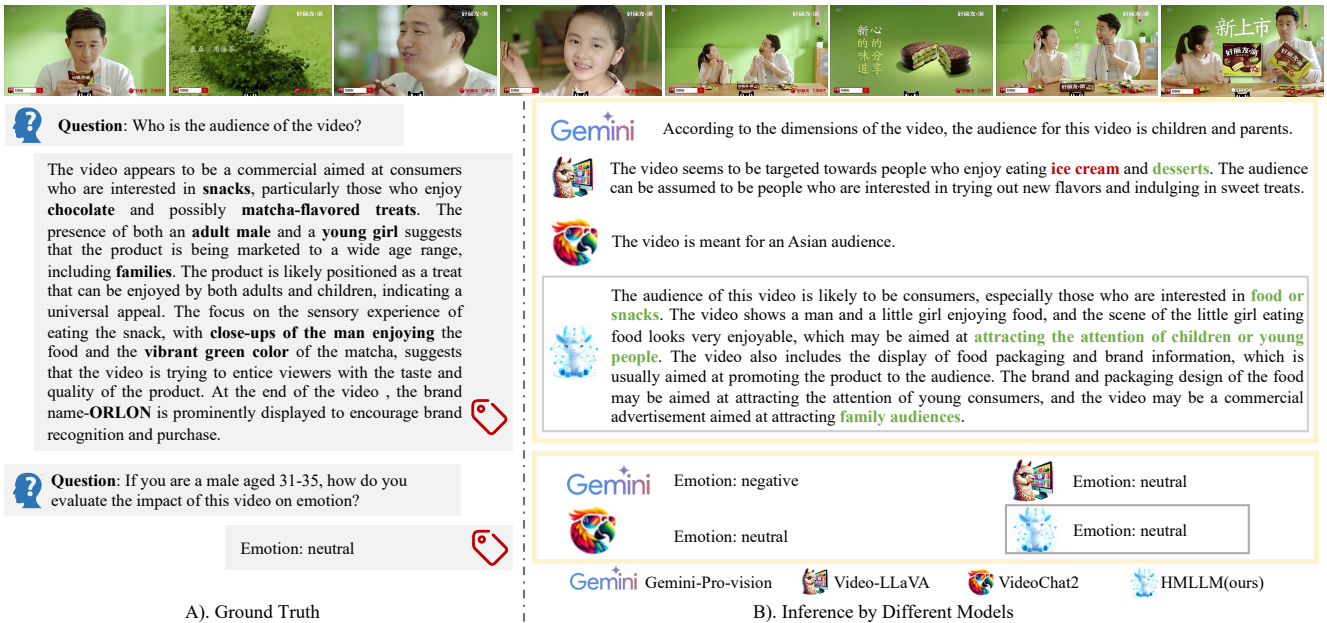


Figure 4. Qualitative analysis of SRI-ADV. Green signifies accurate descriptions, while red denotes incorrect responses.

5.1. Intra Testing

5.1.1 Intra Testing on SRI-ADV

As described in Section 3.4, we have designed two tasks on the collected SRI-ADV dataset, namely Subjectivity and Objectivity.

Subjectivity task. In this task, two protocols are encompassed, *i.e.*, P1, and P2. As shown in Table 3, we present our proposed method HMLLM alongside those from renowned MLLMs such as Gemini-pro-vision, GPT4V, Video-LLaVA, and Video-Chat2. The results, observed

from top to bottom, indicate:

1) For zero-shot inference, GPT4V and Video-LLaVA significantly outperformed the random across-the-board. Gemini-pro-vision underperformed the Random baseline in predicting the accuracy of Engagement and Emotion. Video-Chat2’s failure to follow instructions made it difficult to obtain meaningful results. The settings and prompts of zero-shot inference can be found in the appendix.

2) Upon fine-tuning the models with the SRI-ADV dataset, we observed notable improvements in performance for both Video-LLaVA and Video-Chat2 across both P1 and P2, compared to their initial zero-shot configurations.

Table 4. Comparative performance of different models on the Objectivity task. Using the FSVR strategy is denoted by a "△". The underline of GPT4V denotes the upper bound. We compute the Accuracy (Acc) and VideoChatGPT-Score (Score) [50] of the proposed method HMLLM and other compared state-of-the-art methods on testing data.

Models	Settings	Acc	Score [50]
GPT4V [△]	Zero-shot	<u>84.80</u>	<u>3.99</u>
Gemini-pro-vision [△]	Zero-shot	27.15	2.35
Video-LLaVA [45]	Zero-shot	15.20	2.06
Video-Chat2 [40]	Zero-shot	21.80	2.11
Video-LLaVA [45]	Finetune	44.76	3.03
Video-Chat2 [40]	Finetune	49.27	3.12
HMLLM (Ours)	Finetune	50.52	3.13

Table 5. Results of video conversation benchmark [50]. CI: Correctness of Information, DO: Detail Orientation, CU: Contextual Understanding, TU: Temporal Understanding, C: Consistency.

Models	CI	DO	CU	TU	C	Avg.
Video LLaMA [78]	1.96	2.18	2.16	1.82	1.79	1.98
Video Chat [39]	2.23	2.50	2.53	1.94	2.24	2.29
LLaMA Adapter [79]	2.03	2.32	2.30	1.98	2.15	2.16
Video-ChatGPT [50]	2.40	2.52	2.62	1.98	2.37	2.38
Video-Chat2 [40]	3.02	2.88	3.51	2.66	2.81	2.98
HMLLM (Ours)	3.12	2.86	3.52	2.61	2.91	2.99

Table 6. Results of λ on Proccol2 of the Subjectivity Task.

λ	Engagement		Emotion		EMR	
	ACC	F1	ACC	F1	ACC	F1
0.0	60.06	60.02	39.66	40.24	44.06	45.51
0.05	62.69	63.66	42.62	42.46	52.22	54.78
0.1	64.43	64.65	43.20	48.84	51.96	56.24
0.2	62.38	63.28	38.06	39.79	50.57	50.56
0.5	60.86	60.83	40.17	42.34	50.89	52.47

Moreover, our proposed HMLLM demonstrated the most substantial advancements, consistently outperforming other state-of-the-art methods across all evaluated metrics and protocols.

In detail, within Protocol 1, HMLLM surpassed the leading benchmarks in the categories of Engagement (2 classes), Emotion (3 classes), and EMR Duration (3 classes). The improvements were remarkable, showing enhancements in (accuracy, F1) scores by (3.07, 2.31), (6.08, 2.89), and (1.00, 0.63), respectively. These results underscored the efficacy of our method in accurately capturing and analyzing both engagement and emotional dynamics, as well as predicting EMR duration with high precision. For Protocol 2, the superiority of HMLLM is equally evident. Again, it outshined the best-existing benchmarks in Engagement (2 classes), Emotion (3 classes), and EMR Duration (3 classes), with enhancements in (accuracy, F1) scores by

(4.37, 1.34), (3.54, 4.12), and (7.90, 5.40), respectively. These findings highlight the robustness and adaptability of our model across different protocols, further establishing its potential for widespread applicability in real-world scenarios.

Objectivity Task. In the exploration of the objectivity task, as detailed in Section 3.3, we meticulously refined the ground truth (GT) by manually correcting annotations initially provided by GPT4V. This meticulous process contributed to the notably high zero-shot inference capabilities observed for GPT4V. Given that Gemini-pro-vision and GPT4V inherently lack support for video inputs, we integrated Frame Sequence Video Representation (FSVR) technology to bridge this gap. This adaptation endowed both models with the ability to process video inputs, thus expanding their applicability across a wider range of tasks. As shown in Table 4, GTP4V became the upper bound in a zero-shot setting because we semi-automatically utilized it for labeling, as described in Section 3.3. When the narrative shifts upon the fine-tuning of our models with the SRI-ADV dataset. Both Video-LLaVA and Video-Chat2 showcased substantial enhancements in their performance metrics, surpassing their initial zero-shot configurations. This improvement highlights the transformative impact of targeted training on model efficacy. Notably, our proposed HMLLM method emerged as a formidable contender, eclipsing other models in performance across the board. Specifically, HMLLM outperformed the best baseline, Video-Chat2, in terms of accuracy and the Score [50] by 1.25 and 0.01, respectively.

The results not only validate the effectiveness of fine-tuning with the SRI-ADV dataset but also emphasize that our HMLLM method sets a new benchmark in model performance.

5.1.2 Intra Testing on Video Conversation Benchmark

To further validate the performance of HMLLM, we conducted experiments on other video-based generative performance benchmarks. Following the setup of Video-ChatGPT[50], we present the performance of our proposed HMLLM, detailed in the last row of Table 5. Experimental results demonstrate that the HMLLM effectively enhances both Contextual Understanding and Consistency. Given the HMLLM did not overemphasize temporal details, a slight decrease in Temporal Understanding was observed.

5.2. Ablation Study

Effect of λ . In the course of training HMLLM, a series of ablation studies were carried out on the λ in Equation 7, the results of which are detailed in Table 6. The integration of the SAL-HL Module significantly bolstered the model’s proficiency in capturing subjective metrics, culmi-

nating in optimal performance at a λ value of 0.1. Beyond this threshold, any further increase in λ resulted in a slight decrease in performance, likely due to an overemphasis on SAL-HL features at the expense of the SALM’s inferential capabilities. Despite this, HMLLM consistently surpasses the baseline model ($\lambda = 0.0$) in terms of inference strength, demonstrating the beneficial impact of the hypergraph integration on the model’s overall performance.

5.3. Analysis and Visualization

We further present a qualitative comparison in Figure 6. HMLLM demonstrates an enhanced ability to generate longer and more comprehensive responses for Objectivity Tasks. This improvement can be attributed to the longer average context length of our dataset, which facilitates a deeper understanding of video content by enabling detailed analysis of advertising plots and visual elements. More detailed qualitative analyses are available in the appendix.

6. Conclusion

In this paper, we released a large-scale SRI-ADV dataset with two challenging tasks. We hope it will push cutting-edge research in video understanding. Besides, we proposed a novel HMLLM approach that enhances the language model by constructing a hypergraph feature space across modalities, thereby providing semantically richer associative features. Finally, we conducted a comprehensive set of experiments on both SRI-ADV and other video-based generative datasets, verifying the significance of the proposed dataset and method.

7. Acknowledgments

This work was supported by the Brain-like General Vision Model and Applications project (Grant No. 2022ZD0160403), China Postdoctoral Science Foundation (2023M740079, GZC20230058).

References

- [1] Josh Achiam, Steven Adler, Sandhini Agarwal, Lama Ahmad, Ilge Akkaya, Florencia Leoni Aleman, Diogo Almeida, Janko Altenschmidt, Sam Altman, Shyamal Anadkat, et al. Gpt-4 technical report. *arXiv preprint arXiv:2303.08774*, 2023. 3, 8
- [2] Jean-Baptiste Alayrac, Jeff Donahue, Pauline Luc, Antoine Miech, Iain Barr, Yana Hasson, Karel Lenc, Arthur Mensch, Katherine Millican, Malcolm Reynolds, et al. Flamingo: a visual language model for few-shot learning. *Advances in neural information processing systems*, 35:23716–23736, 2022. 3
- [3] Anurag Arnab, Mostafa Dehghani, Georg Heigold, Chen Sun, Mario Lučić, and Cordelia Schmid. Vivit: A video vision transformer. In *Proceedings of the IEEE/CVF international conference on computer vision*, pages 6836–6846, 2021. 3
- [4] Devanshu Arya, Deepak K Gupta, Stevan Rudinac, and Marcel Worring. Hypersage: Generalizing inductive representation learning on hypergraphs. *arXiv preprint arXiv:2010.04558*, 2020. 3
- [5] David Azcona, Enric Moreu, Feiyan Hu, Tomás E Ward, and Alan F Smeaton. Predicting media memorability using ensemble models. *CEUR Workshop Proceedings*, 2020. 3
- [6] Claude Berge. *Hypergraphs: combinatorics of finite sets*. Elsevier, 1984. 2
- [7] Gedas Bertasius, Heng Wang, and Lorenzo Torresani. Is space-time attention all you need for video understanding? In *ICML*, page 4, 2021. 3
- [8] Gyorgy Buzsaki and Andreas Draguhn. Neuronal oscillations in cortical networks. *science*, 304(5679):1926–1929, 2004. 3
- [9] Huili Cai, Xiaofeng Liu, Rongrong Ni, Siyang Song, and Angelo Cangelosi. Emotion recognition through combining eeg and eog over relevant channels with optimal windowing. *IEEE Transactions on Human-Machine Systems*, 2023. 3
- [10] Joao Carreira and Andrew Zisserman. Quo vadis, action recognition? a new model and the kinetics dataset. In *proceedings of the IEEE Conference on Computer Vision and Pattern Recognition*, pages 6299–6308, 2017. 3
- [11] Yen-Chun Chen, Linjie Li, Licheng Yu, Ahmed El Kholy, Faisal Ahmed, Zhe Gan, Yu Cheng, and Jingjing Liu. Uniter: Universal image-text representation learning. In *European conference on computer vision*, pages 104–120. Springer, 2020. 1
- [12] Wei-Lin Chiang, Zhuohan Li, Zi Lin, Ying Sheng, Zhanghao Wu, Hao Zhang, Lianmin Zheng, Siyuan Zhuang, Yonghao Zhuang, Joseph E Gonzalez, et al. Vicuna: An open-source chatbot impressing gpt-4 with 90%* chatgpt quality. See <https://vicuna.lmsys.org> (accessed 14 April 2023), 2(3):6, 2023. 7
- [13] Romain Cohendet, Claire-Hélène Demarty, Ngoc QK Duong, and Martin Engilberge. Videomem: Constructing, analyzing, predicting short-term and long-term video memorability. In *Proceedings of the IEEE/CVF International Conference on Computer Vision*, pages 2531–2540, 2019. 3

- [14] Mihai Gabriel Constantin, Miriam Redi, Gloria Zen, and Bogdan Ionescu. Computational understanding of visual interestingness beyond semantics: literature survey and analysis of covariates. *ACM Computing Surveys (CSUR)*, 52(2): 1–37, 2019. 3
- [15] Wenliang Dai, Junnan Li, Dongxu Li, Anthony Meng Huat Tiong, Junqi Zhao, Weisheng Wang, Boyang Li, Pascale N Fung, and Steven Hoi. Instructblip: Towards general-purpose vision-language models with instruction tuning. *Advances in Neural Information Processing Systems*, 36, 2024. 3
- [16] Ali Diba, Mohsen Fayyaz, Vivek Sharma, Manohar Paluri, Jürgen Gall, Rainer Stiefelhagen, and Luc Van Gool. Large scale holistic video understanding. In *Computer Vision–ECCV 2020: 16th European Conference, Glasgow, UK, August 23–28, 2020, Proceedings, Part V 16*, pages 593–610. Springer, 2020. 3
- [17] Jeffrey Donahue, Lisa Anne Hendricks, Sergio Guadarrama, Marcus Rohrbach, Subhashini Venugopalan, Kate Saenko, and Trevor Darrell. Long-term recurrent convolutional networks for visual recognition and description. In *Proceedings of the IEEE conference on computer vision and pattern recognition*, pages 2625–2634, 2015. 3
- [18] Victor Escorcia, Fabian Caba Heilbron, Juan Carlos Niebles, and Bernard Ghanem. Daps: Deep action proposals for action understanding. In *Computer Vision–ECCV 2016: 14th European Conference, Amsterdam, The Netherlands, October 11–14, 2016, Proceedings, Part III 14*, pages 768–784. Springer, 2016. 3
- [19] Christoph Feichtenhofer, Axel Pinz, and Andrew Zisserman. Convolutional two-stream network fusion for video action recognition. In *Proceedings of the IEEE conference on computer vision and pattern recognition*, pages 1933–1941, 2016. 3
- [20] Christoph Feichtenhofer, Haoqi Fan, Jitendra Malik, and Kaiming He. Slowfast networks for video recognition. In *Proceedings of the IEEE/CVF international conference on computer vision*, pages 6202–6211, 2019. 3
- [21] Yifan Feng, Haoxuan You, Zizhao Zhang, Rongrong Ji, and Yue Gao. Hypergraph neural networks. In *Proceedings of the AAAI conference on artificial intelligence*, pages 3558–3565, 2019. 3, 7
- [22] Yue Gao, Meng Wang, Dacheng Tao, Rongrong Ji, and Qionghai Dai. 3-d object retrieval and recognition with hypergraph analysis. *IEEE transactions on image processing*, 21(9):4290–4303, 2012. 3
- [23] Yue Gao, Meng Wang, Zheng-Jun Zha, Jialie Shen, Xuelong Li, and Xindong Wu. Visual-textual joint relevance learning for tag-based social image search. *IEEE Transactions on Image Processing*, 22(1):363–376, 2012. 3
- [24] Yue Gao, Zizhao Zhang, Haojie Lin, Xibin Zhao, Shaoyi Du, and Changqing Zou. Hypergraph learning: Methods and practices. *IEEE Transactions on Pattern Analysis and Machine Intelligence*, 44(5):2548–2566, 2020. 3
- [25] Rohit Girdhar, Alaeldin El-Nouby, Zhuang Liu, Mannat Singh, Kalyan Vasudev Alwala, Armand Joulin, and Ishan Misra. Imagebind: One embedding space to bind them all. In *Proceedings of the IEEE/CVF Conference on Computer Vision and Pattern Recognition*, pages 15180–15190, 2023. 3
- [26] Jing Huang and Jie Yang. Unignn: a unified framework for graph and hypergraph neural networks. *arXiv preprint arXiv:2105.00956*, 2021. 3
- [27] Sheng Huang, Mohamed Elhoseiny, Ahmed Elgammal, and Dan Yang. Learning hypergraph-regularized attribute predictors. In *Proceedings of the IEEE conference on computer vision and pattern recognition*, pages 409–417, 2015. 3
- [28] Shaohan Huang, Li Dong, Wenhui Wang, Yaru Hao, Saksham Singhal, Shuming Ma, Tengchao Lv, Lei Cui, Owais Khan Mohammed, Barun Patra, et al. Language is not all you need: Aligning perception with language models. *Advances in Neural Information Processing Systems*, 36, 2024. 3
- [29] HuEdward J., Yulong Shen, Phillip Wallis, Zeyuan Allen-Zhu, Yuanzhi Li, Shean Wang, and Weizhu Chen. Lora: Low-rank adaptation of large language models. *arXiv: Computation and Language, arXiv: Computation and Language*, 2021. 15
- [30] Yunseok Jang, Yale Song, Youngjae Yu, Youngjin Kim, and Gunhee Kim. Tgif-qa: Toward spatio-temporal reasoning in visual question answering. In *2017 IEEE Conference on Computer Vision and Pattern Recognition (CVPR)*, 2017. 1, 2
- [31] Chao Jia, Yinfei Yang, Ye Xia, Yi-Ting Chen, Zarana Parekh, Hieu Pham, Quoc Le, Yun-Hsuan Sung, Zhen Li, and Tom Duerig. Scaling up visual and vision-language representation learning with noisy text supervision. In *International conference on machine learning*, pages 4904–4916. PMLR, 2021. 1
- [32] Cliff Joslyn, Sinan Aksoy, Dustin Arendt, Louis Jenkins, Brenda Praggastis, Emilie Purvine, and Marcin Zalewski. High performance hypergraph analytics of domain name system relationships. In *HICSS 2019 symposium on cybersecurity big data analytics*, 2019. 3
- [33] Nikola Kasabov and Elisa Capecci. Spiking neural network methodology for modelling, classification and understanding of eeg spatio-temporal data measuring cognitive processes. *Information Sciences*, 294:565–575, 2015. 3
- [34] Chamandeep Kaur, Preeti Singh, et al. Eeg derived neuronal dynamics during meditation: Progress and challenges. *Advances in preventive medicine*, 2015, 2015. 5, 14
- [35] Ashmit Khandelwal, Aditya Agrawal, Aanisha Bhat-tacharyya, Yaman K Singla, Somesh Singh, Uttaran Bhat-tacharya, Ishita Dasgupta, Stefano Petrangeli, Rajiv Ratn Shah, Changyou Chen, et al. Large content and behavior models to understand, simulate, and optimize content and behavior. *arXiv preprint arXiv:2309.00359*, 2023. 2
- [36] Wolfgang Klimesch. Eeg alpha and theta oscillations reflect cognitive and memory performance: a review and analysis. *Brain research reviews*, 29(2-3):169–195, 1999. 5, 14
- [37] Jing Yu Koh, Ruslan Salakhutdinov, and Daniel Fried. Grounding language models to images for multimodal generation. *arXiv preprint arXiv:2301.13823*, 2, 2023. 3
- [38] Junnan Li, Dongxu Li, Silvio Savarese, and Steven Hoi. Blip-2: Bootstrapping language-image pre-training with

- frozen image encoders and large language models. In *International conference on machine learning*, pages 19730–19742. PMLR, 2023. 3, 6, 7
- [39] KunChang Li, Yinan He, Yi Wang, Yizhuo Li, Wenhai Wang, Ping Luo, Yali Wang, Limin Wang, and Yu Qiao. Videochat: Chat-centric video understanding. *arXiv preprint arXiv:2305.06355*, 2023. 3, 9
- [40] Kunchang Li, Yali Wang, Yinan He, Yizhuo Li, Yi Wang, Yi Liu, Zun Wang, Jilan Xu, Guo Chen, Ping Luo, Limin Wang, and Yu Qiao. Mvbench: A comprehensive multimodal video understanding benchmark, 2023. 8, 9, 15
- [41] Kunchang Li, Yali Wang, Yizhuo Li, Yi Wang, Yinan He, Limin Wang, and Yu Qiao. Unmasked teacher: Towards training-efficient video foundation models, 2023. 7
- [42] Mingcheng Li, Dingkan Yang, and Lihua Zhang. Towards robust multimodal sentiment analysis under uncertain signal missing. *IEEE Signal Processing Letters*, 2023. 3
- [43] Xiujun Li, Xi Yin, Chunyuan Li, Pengchuan Zhang, Xiaowei Hu, Lei Zhang, Lijuan Wang, Houdong Hu, Li Dong, Furu Wei, et al. Oscar: Object-semantics aligned pre-training for vision-language tasks. In *Computer Vision–ECCV 2020: 16th European Conference, Glasgow, UK, August 23–28, 2020, Proceedings, Part XXX 16*, pages 121–137. Springer, 2020. 1
- [44] Yangguang Li, Feng Liang, Lichen Zhao, Yufeng Cui, Wanli Ouyang, Jing Shao, Fengwei Yu, and Junjie Yan. Supervision exists everywhere: A data efficient contrastive language-image pre-training paradigm. *arXiv preprint arXiv:2110.05208*, 2021. 1
- [45] Bin Lin, Bin Zhu, Yang Ye, Munan Ning, Peng Jin, and Li Yuan. Video-llava: Learning united visual representation by alignment before projection. *arXiv preprint arXiv:2311.10122*, 2023. 3, 8, 9
- [46] Tianwei Lin, Xu Zhao, and Zheng Shou. Single shot temporal action detection. In *Proceedings of the 25th ACM international conference on Multimedia*, pages 988–996, 2017. 3
- [47] Haotian Liu, Chunyuan Li, Qingyang Wu, and Yong Jae Lee. Visual instruction tuning. *Advances in neural information processing systems*, 36, 2024. 3
- [48] Qingshan Liu, Yubao Sun, Cantian Wang, Tongliang Liu, and Dacheng Tao. Elastic net hypergraph learning for image clustering and semi-supervised classification. *IEEE Transactions on Image Processing*, 26(1):452–463, 2016. 3
- [49] Wolfgang Maass. Networks of spiking neurons: the third generation of neural network models. *Neural networks*, 10(9):1659–1671, 1997. 3
- [50] Muhammad Maaz, Hanoona Rasheed, Salman Khan, and Fahad Shahbaz Khan. Video-chatgpt: Towards detailed video understanding via large vision and language models. *arXiv:2306.05424*, 2023. 1, 2, 5, 7, 9
- [51] Daniel Neimark, Omri Bar, Maya Zohar, and Dotan Asseilmann. Video transformer network. In *Proceedings of the IEEE/CVF international conference on computer vision*, pages 3163–3172, 2021. 3
- [52] Anelise Newman, Camilo Fosco, Vincent Casser, Allen Lee, Barry McNamara, and Aude Oliva. Multimodal memorability: Modeling effects of semantics and decay on video memorability. In *Computer Vision–ECCV 2020: 16th European Conference, Glasgow, UK, August 23–28, 2020, Proceedings, Part XVI 16*, pages 223–240. Springer, 2020. 3
- [53] Long Ouyang, Jeffrey Wu, Xu Jiang, Diogo Almeida, Carroll Wainwright, Pamela Mishkin, Chong Zhang, Sandhini Agarwal, Katarina Slama, Alex Ray, et al. Training language models to follow instructions with human feedback. *Advances in neural information processing systems*, 35:27730–27744, 2022. 3
- [54] Jikai Pan, Shangfei Wang, and et. al. Representation learning through multimodal attention and time-sync comments for affective video content analysis. In *Proceedings of the 30th ACM International Conference on Multimedia*, pages 42–50, 2022. 3
- [55] Edmund T Rolls. *The brain, emotion, and depression*. Oxford University Press, 2018. 2
- [56] Yannick Roy, Hubert Banville, Isabela Albuquerque, Alexandre Gramfort, Tiago H Falk, and Jocelyn Faubert. Deep learning-based electroencephalography analysis: a systematic review. *Journal of neural engineering*, 16(5): 051001, 2019. 2
- [57] J. A. Russell. A circumplex model of affect. *Journal of Personality and Social Psychology*, 39:1161–1178, 1980. 3
- [58] Karen Simonyan and Andrew Zisserman. Two-stream convolutional networks for action recognition in videos. *Advances in neural information processing systems*, 27, 2014. 3
- [59] Tengfei Song, Wenming Zheng, Peng Song, and Zhen Cui. Eeg emotion recognition using dynamical graph convolutional neural networks. *IEEE Transactions on Affective Computing*, 11(3):532–541, 2020. 3
- [60] Xiaolin Song, Qiaoju Kang, Zekun Tian, Yi Yang, Sihao Yang, Qiang Gao, and Yu Song. Eeg-based emotion classification with wavelet entropy feature. In *2020 Chinese Automation Congress (CAC)*, pages 5685–5689, 2020. 3
- [61] Yixuan Su, Tian Lan, Huayang Li, Jialu Xu, Yan Wang, and Deng Cai. Pandagpt: One model to instruction-follow them all. *arXiv preprint arXiv:2305.16355*, 2023. 3
- [62] Abdulhamit Subasi, Turker Tuncer, Sengul Dogan, Dahiru Tanko, and Unal Sakoglu. Eeg-based emotion recognition using tunable q wavelet transform and rotation forest ensemble classifier. *Biomedical Signal Processing and Control*, 68: 102648, 2021. 14
- [63] Gemini Team, Rohan Anil, Sebastian Borgeaud, Yonghui Wu, Jean-Baptiste Alayrac, Jiahui Yu, Radu Soricut, Johan Schalkwyk, Andrew M Dai, Anja Hauth, et al. Gemini: a family of highly capable multimodal models. *arXiv preprint arXiv:2312.11805*, 2023. 8
- [64] S Vajda. The mathematical theory of communication. by claud e. shannon and warren weaver. pp. 117. 1949. *The Mathematical Gazette*, 34(310):312–313, 1950. 2
- [65] Jianfeng Wang, Zhengyuan Yang, Xiaowei Hu, Linjie Li, Kevin Lin, Zhe Gan, Zicheng Liu, Ce Liu, and Lijuan Wang. Git: A generative image-to-text transformer for vision and language. *arXiv preprint arXiv:2205.14100*, 2022. 3
- [66] Limin Wang, Yuanjun Xiong, Zhe Wang, Yu Qiao, Dahua Lin, Xiaoou Tang, and Luc Van Gool. Temporal segment networks: Towards good practices for deep action recognition.

- In *European conference on computer vision*, pages 20–36. Springer, 2016. 3
- [67] Meng Wang, Xueliang Liu, and Xindong Wu. Visual classification by hypergraph modeling. *IEEE Transactions on Knowledge and Data Engineering*, 27(9):2564–2574, 2015. 3
- [68] Xianyuan Wang, Zhenjiang Miao, Ruyi Zhang, and Shanshan Hao. I3d-lstm: A new model for human action recognition. In *IOP conference series: materials science and engineering*, page 032035. IOP Publishing, 2019. 3
- [69] Jason Wei, Yi Tay, Rishi Bommasani, Colin Raffel, Barret Zoph, Sebastian Borgeaud, Dani Yogatama, Maarten Bosma, Denny Zhou, Donald Metzler, et al. Emergent abilities of large language models. *arXiv preprint arXiv:2206.07682*, 2022. 1
- [70] Shengqiong Wu, Hao Fei, Leigang Qu, Wei Ji, and Tat-Seng Chua. Next-gpt: Any-to-any multimodal llm. *arXiv preprint arXiv:2309.05519*, 2023. 3
- [71] Xun Wu, Wei-Long Zheng, Ziyi Li, and Bao-Liang Lu. Investigating eeg-based functional connectivity patterns for multimodal emotion recognition. *Journal of neural engineering*, 19(1):016012, 2022. 3
- [72] Dejing Xu, Zhou Zhao, Jun Xiao, Fei Wu, Hanwang Zhang, Xiangnan He, and Yueting Zhuang. Video question answering via gradually refined attention over appearance and motion. In *ACM Multimedia*, 2017. 1, 2
- [73] Naganand Yadati, Madhav Nimishakavi, Prateek Yadav, Vikram Nitin, Anand Louis, and Partha Talukdar. Hypergcn: A new method for training graph convolutional networks on hypergraphs. *Advances in neural information processing systems*, 32, 2019. 3
- [74] Wilson Yan, Yunzhi Zhang, Pieter Abbeel, and Aravind Srinivas. Videogpt: Video generation using vq-vae and transformers. *arXiv preprint arXiv:2104.10157*, 2021. 3
- [75] Qinghao Ye, Haiyang Xu, Guohai Xu, Jiabo Ye, Ming Yan, Yiyang Zhou, Junyang Wang, Anwen Hu, Pengcheng Shi, Yaya Shi, et al. mplug-owl: Modularization empowers large language models with multimodality. *arXiv preprint arXiv:2304.14178*, 2023. 3
- [76] Zhou Yu, Dejing Xu, Jun Yu, Ting Yu, Zhou Zhao, Yueting Zhuang, and Dacheng Tao. Activitynet-qa: A dataset for understanding complex web videos via question answering. In *AAAI*, pages 9127–9134, 2019. 1, 2
- [77] Dong Zhang, Shimin Li, Xin Zhang, Jun Zhan, Pengyu Wang, Yaqian Zhou, and Xipeng Qiu. Speechgpt: Empowering large language models with intrinsic cross-modal conversational abilities. *arXiv preprint arXiv:2305.11000*, 2023. 3
- [78] Hang Zhang, Xin Li, and Lidong Bing. Video-llama: An instruction-tuned audio-visual language model for video understanding. *arXiv preprint arXiv:2306.02858*, 2023. 3, 9
- [79] Renrui Zhang, Jiaming Han, Chris Liu, Peng Gao, Aojun Zhou, Xiangfei Hu, Shilin Yan, Pan Lu, Hongsheng Li, and Yu Qiao. Llama-adapter: Efficient fine-tuning of language models with zero-init attention. *arXiv preprint arXiv:2303.16199*, 2023. 9
- [80] Zizhao Zhang, Haojie Lin, Xibin Zhao, Rongrong Ji, and Yue Gao. Inductive multi-hypergraph learning and its application on view-based 3d object classification. *IEEE Transactions on Image Processing*, 27(12):5957–5968, 2018. 3
- [81] Zhicheng Zhang, Lijuan Wang, and Jufeng Yang. Weakly supervised video emotion detection and prediction via cross-modal temporal erasing network. In *CVPR 2023*, pages 18888–18897, 2023. 3
- [82] Tony Zhao, Irving Fang, Jeffrey Kim, and Gerald Friedland. Multi-modal ensemble models for predicting video memorability. *arXiv preprint arXiv:2102.01173*, 2021. 3
- [83] Yue Zhao, Yuanjun Xiong, Limin Wang, Zhirong Wu, Xiaoou Tang, and Dahua Lin. Temporal action detection with structured segment networks. In *Proceedings of the IEEE international conference on computer vision*, pages 2914–2923, 2017. 3
- [84] Deyao Zhu, Jun Chen, Xiaoqian Shen, Xiang Li, and Mohamed Elhoseiny. Minigt-4: Enhancing vision-language understanding with advanced large language models. *arXiv preprint arXiv:2304.10592*, 2023. 3

A. Analysis of EEG Raw Signal

Electroencephalography (EEG) stands as a pivotal method for recording the electrical activity of the brain. This is achieved through the placement of electrodes across the scalp, shown in Figure 5, to detect electrical signals from neurons. These signals are instrumental in delineating the brain’s activity patterns across various cognitive states, providing deep insights into how the brain orchestrates complex psychological emotions and cognitive processes.

EEG signals are characterized by multiple frequency bands, among which Alpha and Beta waves are paramount, each corresponding to distinct functional states of the brain [34, 36, 62]. We categorize different EEG bands according to the following frequency definitions:

- Alpha Waves (8–13 Hz) are emblematic of the brain’s state of relaxation and idleness. They are further categorized into three sub-bands based on their frequency range. 1) Alpha1 (8–8.9 Hz): This band is predominant when an individual is in a relaxed state with closed eyes, marking the onset of relaxation. 2) Alpha2 (9–10.9 Hz): These waves are more pronounced when the individual is relaxed yet maintains a level of alertness. 3) Alpha3 (11–12.9 Hz): This band appears as the brain relaxes further while remaining somewhat awake.
- Beta waves (13–30 Hz) are integral to the brain’s alertness, focused attention, and cognitive processing. 1) Beta1 (13–18 Hz): Associated with mild cognitive activities and focused attention, like reading or simple thought processes. 2) Beta2 (18–22 Hz): These waves intensify during complex cognitive tasks such as problem-solving and decision-making. 3) Beta3 (22–30 Hz): This range signifies highly focused attention and rapid cognitive processing, indicative of active information processing.

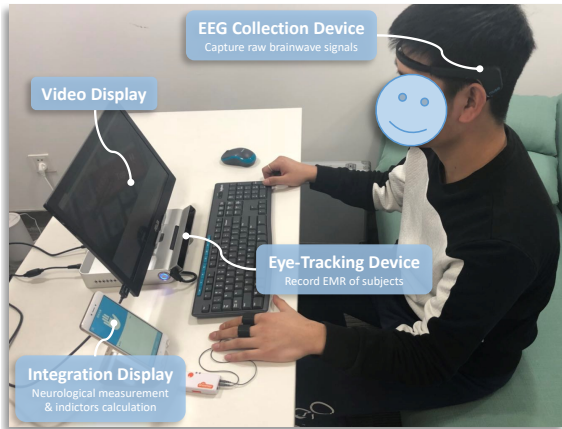


Figure 5. Equipment for Collecting Subjective Responses of SRI-ADV dataset. During data acquisition, participants wear an EEG Device, facing a Video Display, with an Eye-Tracking Device below to monitor gaze. Video durations and subjective responses are recorded on an Integration Display for analysis.

Table 7. Categories & Distribution of Subjectivity Task

Task	Engagement	Emotion	EMR
Cls-1	non-cognitive [0, 1) prop. 55.0%	negative ($-\infty, -6$) prop. 29.7%	not attended [0, 0.45) prop. 29.3%
Cls-2	cognitive [1, $+\infty$) prop. 45.0%	neutral ($-6, 6$) prop. 39.0%	partially attended [0.45, 0.6) prop. 41.6%
Cls-3	–	positive ($6, +\infty$) prop. 31.2%	fully attended [0.6, $+\infty$) prop. 29.0%
Distri.			

In this research, we analyze EEG signals and eye movement metrics to capture authentic subjective feedback from diverse demographic groups in response to advertisements. The SRI-ADV dataset, derived from raw signals and specific frequency bands, aids in improving the understanding of videos, especially those related to advertising.

B. Data distribution of Subjectivity Task in SRI-ADV

We initiate our analysis by performing a comprehensive histogram distribution assessment of Engagement, Emotion, and EMR indicators, anchored to Audience Profiles benchmarks. As delineated in Table 7, the concluding row graphically encapsulates the distribution of each evaluated SRI. The table’s initial three rows delineate each category’s designation, value range, and the proportion of data attributed to the corresponding category. For instance, the Engagement indicator is bifurcated into two categories: the first, termed “non-cognitive,” spans a value range from 0 to 1 (non-inclusive), with 55.0% of observations classified under this category.

Leveraging the statistical insights derived, we proceed to discretize the extant SRI values into distinct categories, thereby facilitating the structuring of the Subjectivity Task associated with SRI-ADV.

C. Method Algorithm and Training Hyperparameters

We introduce the Hypergraph Multimodal Large Language Model (HMLLM), a novel approach designed to integrate and process multi-modal data, taking into full account both subjective and objective elements to comprehend advertising videos. Our training procedure is detailed in Algorithm 1. The method is grounded in the utilization of hypergraphs and large language model to effectively handle complex relationships within and across modalities.

We divide the training process into the following stages and adapt appropriate training hyperparameters, as shown in Table 8.

Algorithm 1: HMLLM: Hypergraph Multi-modal Large Language Model

Input : Video Key Frames $F = \{f_0, f_1, \dots, f_N\}$,
Textual Prompts T ,
Ground Truth \mathbf{Y}_{gt} ,
Warm Up Epoch E_0 ,
Fine-tune Epoch E_1 ,

Initialization: $\mathbf{X}_0 \leftarrow \text{Pre_process}(F_v)$
 $\mathbf{F}_v \leftarrow \text{Visual_Encoder}(\mathbf{X}_0)$
 $\text{SALM} \leftarrow \text{Initialize_SALM}(\mathbf{F}_v, T)$
HL-Gate $\leftarrow \text{OFF}$
 $\mathbf{Q} \leftarrow \text{Initialize_Query}()$

// Stage I: SALM Warm Up

- 1 for $i \leftarrow 1$ to E_0 do
- 2 $\mathbf{K}, \mathbf{V} \leftarrow \text{QFormer}(\mathbf{F}_v)$
- 3 $\mathbf{F}_p \leftarrow \text{SALM_Projector}(\mathbf{F}_v, \mathbf{K}, \mathbf{V})$
- 4 $\text{SALM} \leftarrow \text{SALM_Train}(\text{SALM}, \mathbf{F}_p, T)$
- 5 $\tilde{\mathcal{Y}}_{qa} \leftarrow \text{SALM}(\mathbf{F}_p, T)$
- 6 $\mathcal{L}_{ITG} \leftarrow \text{ITG_Loss}(\tilde{\mathcal{Y}}_{qa}, \mathbf{Y}_{gt})$
- 7 $\text{SALM_Optimizer}(\mathcal{L}_{ITG})$

// Stage II: SAL-HL Fine-tuning

- 8 HL-Gate $\leftarrow \text{SRI_Contained}(T)$ // Set HL-Gate ON.
- 9 for $i \leftarrow 1$ to E_1 do
- 10 $\mathbf{F}_{pv} \leftarrow \text{Feature_Mixer}(\mathbf{F}_p, \mathbf{F}_v)$
- 11 $\mathbf{F}_{frame.level} \leftarrow \text{Pool}(\mathbf{F}_{pv})$
- 12 $\mathcal{G} \leftarrow \text{Construct_Hypergraph}(\mathbf{F}_{frame.level}, \mathcal{R})$
- 13 $\tilde{\mathcal{Y}}_{sri} \leftarrow \text{HGNN}(\mathcal{G}, \mathbf{F}_{frame.level})$
- 14 $\mathcal{L}_{CE} \leftarrow \text{Cross_Entropy}(\tilde{\mathcal{Y}}_{sri}, \mathcal{Y}_{sri})$
// \mathcal{L}_{ITG} is obtained same with the stage I
- 15 $\mathcal{L} \leftarrow \text{Combined_Loss}(\mathcal{L}_{ITG}, \mathcal{L}_{CE}, \lambda)$
- 16 $\text{Joint_Optimizer}(\text{SALM}, \text{HGNN}, \mathcal{L})$

C.1. Initialization for Model Parameters

The process begins with the extraction of key frames from the input video, which are then pre-processed to standardize the input format. These initial visual features are encoded using a visual encoder, producing a set of feature vectors. Simultaneously, textual prompts are prepared for processing. A query set is initialized, marking the starting point for our model’s learning process.

C.2. Stage I: SALM Warm Up

Stage I is dedicated to the training of the SRI-Aware Language Model (SALM), with the goal of enhancing its capabilities in language generation and reasoning inference. In this stage, visual features are converted into key-value pairs using a query-former mechanism, essential for the attention processes. These features are then fed through the SALM projector, which enriches the model’s understanding by integrating textual prompts.

The training of SALM spans 10 epochs, as detailed in Table 8, with a particular focus on minimizing the Image-Text Grounding (ITG) loss. This step is crucial for ensuring that the model’s outputs are in alignment with the ground truth, thereby optimizing performance.

C.3. Stage II: SAL-HL Fine-tuning

Stage II shifts the focus to fine-tuning the SRI-Aware Language Hypergraph Learning (SAL-HL) component, with the objective of enhancing the model’s capability to mimic the subjective perceptual capacities of the brain. After completing the initial warm-up phase, the model enters the fine-tuning stage, marked by the activation of the Hypergraph Learning (HL) gate. This process enriches the model’s multi-modal context by combining these features into a pooled frame-level representation. This representation then forms the foundation for constructing a hypergraph that captures the intricate interconnections among data points.

Following the construction of the hypergraph, a Hypergraph Neural Network (HGNN) is employed to process the hypergraph structure, allowing the model to leverage the complex connections present within the data. The output generated by the HGNN is fine-tuned using Cross-Entropy loss along with the Image-Text Grounding (ITG) loss emphasized during the warm-up phase. This amalgamation of loss functions serves as a directive for the optimization process, targeting both the SRI-Aware Language Model (SALM) and the HGNN components. This strategic approach ensures a unified and coherent learning experience throughout the two distinct stages of the model’s training, fostering a comprehensive understanding and adaptation to the intricacies of the data.

Following [40], we incorporate Low-Rank Adaptation (LoRA) [29] modules into the SALM with a configuration of rank 16, an alpha value of 32, and a dropout rate of 0.1 during Stage II. Within the HGNN, it is imperative to adjust the input based on pooled frame-level representation, setting the Number of Vertices and Hyperedges to 8×98 and the Channel of Vertex Representation to 1024. For the hypergraph’s internal configuration, we adhere to the commonly used settings as illustrated in the Table 8, ensuring a balance between training effectiveness and model size.

Table 8. Training Hyperparameters for different stages.

config	Stage1	Stage2
	SALM Warm Up	SAL-HL Fine-tune
input frame	8	
input resolution	224	
max text length	512	
optimizer	AdamW	
optimizer momentum	$\beta_1, \beta_2 = 0.9, 0.999$	
weight decay	0.02	
learning rate schedule	cosine decay	
learning rate	1e-4	2e-5
batch size	128	64
warmup epochs	0.5	1
total epochs	10	20
λ of \mathcal{L}	0	0.1
augmentation	flip, MultiScaleCrop [0.5, 1]	
Vertices number of Hypergraph	-	8*98
Hyperedges number of Hypergraph	-	8*98
Channel of Vertex representation	-	1024
K of hypergraph construction	-	3, 4, 5
Average out-degree of vertices	-	12.5
In-degree of hyperedges	-	3, 4, 5

C.4. Summary

HMLLM stands as a comprehensive framework that leverages the strengths of hypergraph structures and multi-modal data integration. Through its two-stage training process, it achieves a deep understanding of the relationships within and across modalities, paving the way for advanced applications in multi-modal data processing and generation.

D. Computational Complexity and Resource Utilization of HMLLM

We have recorded the training time on eight A100 GPUs, each with 40GB of memory, and the inference time on a single A100 GPU with the same specifications. Our proposed HMLLM is generally on par with other models supporting video multi-modalities in terms of parameter count, training time, and inference time.

Table 9. Comparative Analysis of Model Parameters

Model	Video-Chat2	HMLLM (Ours)
Total Parameters (Billions)	7.2	7.2
Training Time (H/Epoch)	13.5	14.3
Inference Time (s/Video)	6.2	6.2
ACC on Task2	49.27	50.52

E. Zero-shot Prompt for Subjectivity Task

For the subjectivity task, we conducted Zero-shot inference on commercial and open-source models. During this pro-

cess, we tested various Prompts^{2 3} to enable reasoning by the language models. The Prompts we selected are as follows.

As an AI model simulating EEG indicator analysis, your task is to systematically evaluate a user's feelings after viewing video or frames content using the provided EEG indicators: Cognitive Engagement (CE), Emotional Recognition (ER), and Eye Movement Ratio (EMR).

Effective analysis requires detailed video content information themes, narrative structure, visual and auditory elements and viewer attributes, including age, gender, preferences, and experiences. You will integrate the EEG indicators' definitions and probabilities to deduce the viewer's cognitive engagement, emotional response, and attention level.

This involves assessing how video elements may attract or repel the viewer, grounded in psychological principles and media consumption research. But you don't need to output the reasoning process, only the final result.

1. Cognitive Engagement (CE) Definitions:

- A. Non-Cognition:(55% probability)The viewer shows minimal interest or understanding, resulting in low EEG activity.

- B. Cognition:(45% probability)The viewer understands and relates to the video, evidenced by increased EEG activity.

2. Emotional Recognition (ER) Definitions:

- A. Negative:(30% probability)Dislikes certain video elements (e.g., conflict, unappealing objects).

- B. Neutral:(40% probability)Feels indifferent towards the video content (e.g., mundane tasks).

- C. Positive:(30% probability)Experiences enjoyment or excitement (e.g., appealing scenes).

3. Eye Movement Ratio (EMR) Definitions:

- A. Not Attended:(30% probability)Viewing ratio ≤ 0.45 , possibly due to unattractive visuals or cognitive dissonance.

- B. Partially Attended:(40% probability)Viewing ratio between 0.45 and 0.6, suggesting some attractive elements.

- C. Fully Attended:(30% probability)Viewing ratio > 0.6 , indicating high appeal and mood enhancement.

Please ensure your analysis follows this format with no additional output:

CE: B;

ER: B;

EMR: C

²<https://clickup.com/blog/ai-prompt-templates/>

³<https://www.zdnet.com/article/how-to-write-better-chatgpt-prompts-in-5-steps/>

based on probabilities.

{[The Question in Test Set]}

It is worth noting that to prevent the model from overfitting to specific choices, we randomized the options and tested them three times, taking the average result as the conclusive outcome.

F. Visualization and Qualitative Analysis

In the realm of advertising, the use of metaphors, scenic portrayals, and related content is prevalent. Our SRI-ADV dataset is meticulously crafted to support both subjective and objective analyses, thereby offering a comprehensive understanding of video advertising content. It uniquely bridges the gap between these analyses, with objective comprehension bolstering subjective interpretation. This fusion enables the exploration of qualitative aspects such as Engagement, Emotion, and Eye Movement Ratio (EMR) across various demographics.

As shown in Figure 6, Part A showcases the SRI-ADV's ground truth, distinguished by its detailed annotations and extensive response lengths. Meanwhile, Part B delineates a comparative analysis among the outputs generated by the Gemini-Pro-vision, Video-LLaVA, and VideoChat2 models against our HMLLM.

For instance, an energy drink advertisement as shown in the bottom of Figure 6, HMLLM uniquely captures both the overt (a motorcycle rider and a camel) and the covert (the product's essence of vitality and adventure) elements of the advertisement. This comprehensive analysis extends to the advertisement's main audience, design principles, visual narratives, and product attributes, showcasing our model's superior capability in extracting and interpreting complex thematic elements.